CrossMark

Inkjet-Printed In-Ga-Zn Oxide Thin-Film Transistors with Laser Spike Annealing

HANG HUANG,[1] HAILONG HU [ID],[1,2] JINGGUANG ZHU,[1]
and TAILIANG GUO[1]

1.—College of Physics and Information Engineering, Fuzhou University, Fuzhou 350002, China.
2.—e-mail: huhl@fzu.edu.cn

Inkjet-printed In-Ga-Zn oxide (IGZO) thin-film transistors (TFTs) have been fabricated at low temperature using laser spike annealing (LSA) treatment. Coffee-ring effects during the printing process were eliminated to form uniform IGZO films by simply increasing the concentration of solute in the ink. The impact of LSA on the TFT performance was studied. The field-effect mobility, threshold voltage, and on/off current ratio were greatly influenced by the LSA treatment. With laser scanning at 1 mm/s for 40 times, the 30-nm-thick IGZO TFT baked at 200°C showed mobility of 1.5 cm^2/V s, threshold voltage of -8.5 V, and on/off current ratio $> 10^6$. Our findings demonstrate the feasibility of rapid LSA treatment of low-temperature inkjet-printed oxide semiconductor transistors, being comparable to those obtained by conventional high-temperature annealing.

Key words: Indium-gallium-zinc oxide, low temperature, inkjet printing, laser spike annealing, thin-film transistors

INTRODUCTION

Thin-film transistors (TFTs) are one of the most important basic components in active matrix displays. Amorphous indium-gallium-zinc oxide (a-IGZO) TFTs have attracted considerable attention in the last decade due to their excellent properties such as high optical transparency, high electron mobility, superior uniformity, and chemical stability,[1–3] and are considered to be one of the most promising candidates for use in next-generation flexible and transparent flat-panel displays.[4–6] There are various process technologies to fabricate IGZO TFTs, including magnetron sputtering,[7] pulsed laser deposition,[4] spin-coating,[8] and inkjet printing (IJP).[9,10] Among these, inkjet printing is particularly attractive because of low material waste, direct patterning deposition of functional materials, and applicability to large-area devices.[11] As a solution-based process, however, IJP usually requires annealing at high temperature above 400°C to remove organic residues and promote

decomposition and oxidation,[12] which it is not compatible with flexible substrates. For this reason, many researchers have sought alternative annealing techniques with lower process temperature, including precursor engineering,[13] dual active layer,[14] self-combustion reaction,[15] O_2/O_3 annealing,[16] microwave- or ultraviolet (UV)-assisted annealing,[17,18] and high-pressure annealing.[19]

Recently, laser spike annealing (LSA) was used to improve the performance of TFTs.[20] LSA allows one to raise the temperature in a very short time at a specific location by scanning a laser source, without causing thermal damage to the underlying substrate due to rapid quenching.[21,22] So far, this intriguing approach has rarely been applied to IJP transparent oxide TFTs. In this work, we used near-infrared (NIR, $\lambda = 1064$ nm) LSA to anneal IJP-IGZO TFTs, because this laser has greater heating depth in annealed films and higher transmittance, especially for transparent substrates, compared with excimer lasers. After the LSA process, the characteristics of the IGZO TFT were improved significantly, approximating those of TFTs formed using conventional thermal annealing (CTA) at
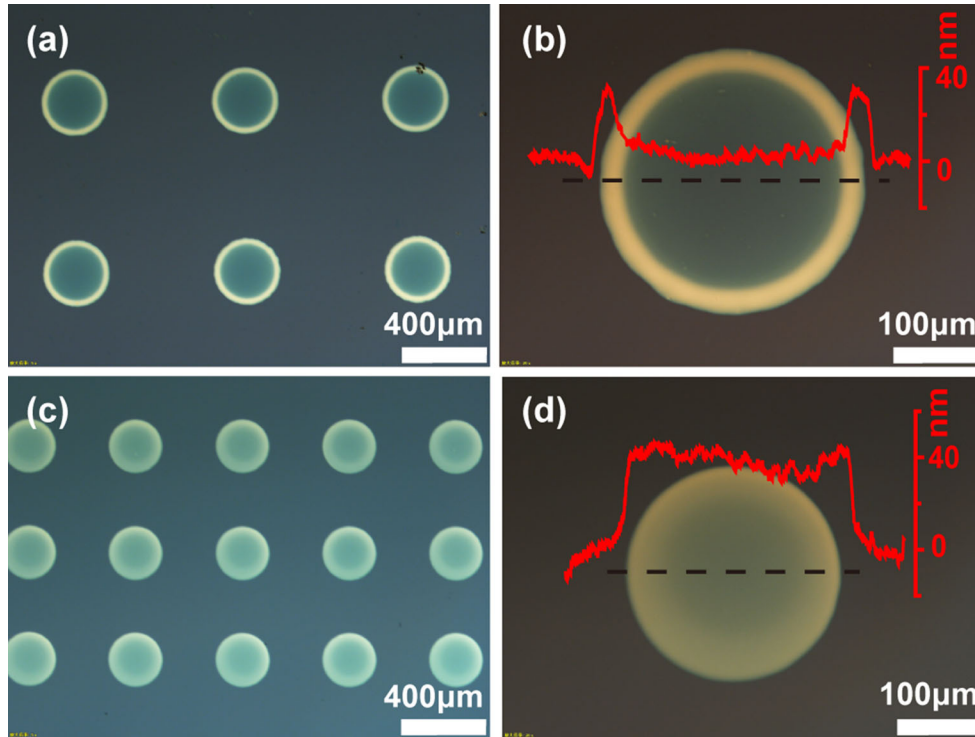
Fig. 1. Optical microscopy images of inkjet-printed dots on SiO$_2$/Si substrate obtained with precursor solution of (a, b) 0.375 M and (c, d) 1.5 M. Insets show surface profiles of printed dots.

Table I. Comparison of coffee-ring phenomenon between various works

Ink	Stabilizing agent	Modulating method	Peak-to-valley height (nm)
IGZO	–	Ink concentration	0–27
ZTO[27]	Ethanolamine	Substrate temperature	60–170
ZTO[27]	Ethanolamine	Surface modification	Dome shape
IGZO[28]	Ethanolamine	Substrate temperature	Dome shape
ZTO[29]	Acetylacetone	Substrate temperature	50–80
In$_2$O$_3$[30]	–	Substrate temperature	10–30

Table II. Viscosity and surface tension (25.4°C) of inks

Ink	Viscosity (mPa s)	Surface tension (dyn/cm)
1.5 M IGZO	8.14	33.4
0.375 M IGZO	2.52	31.4
2ME solvent	1.54	30.8

400°C. As the only heat treatment, i.e., the prebaking process, is conducted at temperature as low as 200°C, this method also shows potential for application on flexible substrates.

EXPERIMENTAL PROCEDURES

IGZO ink was prepared by dissolving zinc acetate dihydrate [Zn(CH$_3$COO)$_2$·2H$_2$O, 99.99%, Aladdin], indium nitrate hydrate [In(NO$_3$)$_3$·H$_2$O, 99.99%, Aladdin], and gallium nitrate hydrate [Ga(NO$_3$)$_3$·H$_2$O, 99.99%, Aladdin] in 2-methoxyethanol [2ME, >99.5%, Aladdin] at molar ratio of 10:63:27 (Ga:In:Zn).[8] The solution was stirred for 3 h at room temperature and filtered using a 0.22-μm polytetrafluoroethylene microfilter. IGZO TFTs were fabricated with a bottom-gate top-contact configuration. A heavily doped p^+-Si wafer (100) was employed as bottom gate with an Al back-contact, while a thermally grown 100-nm-thick SiO$_2$

layer was used as gate dielectric. Before printing, the SiO_2 surface was washed with ethanol and deionized water, and treated by oxygen plasma for 4 min at room temperature. IGZO ink was jetted using a drop-on-demand piezoelectric IJP system (MicroFab Jetlab2) with a 60-μm nozzle at pulse frequency of 1000 Hz in ambient conditions. The printed thin film was prebaked at 200°C in air for 3 h on a hot plate. For LSA, the IGZO films were irradiated by a laser with beam spot size of 30 μm in ambient air. The dwell time and pulse repetition rate of the laser were 15 ns and 300 kHz, respectively. The laser spot was scanned line by line at 1 mm/s to completely cover the printed film. For extended irradiation, multiple scans were conducted by rescanning the surface repeatedly. Finally, 50 nm of Au was deposited by thermal evaporation using a mask for the source and drain electrodes, with channel width and length of 250 μm and 50 μm, respectively. No back passivation was used.

Fig. 2. XPS spectra of IGZO thin films after different treatments.

The viscosity and surface tension of the precursor solutions were characterized by viscometer (Brookfield DV2T) and automatic surface interfacial tensiometer (BZY-1). The thickness and surface morphology of the inkjet-printed IGZO thin films were evaluated by surface profilometer (Alpha-Step D-100), optical microscope (Olympus BX51M), field-emission scanning electron microscopy (FE-SEM, FEI, Nova NanoSEM 230), and atomic force microscopy (AFM, Bruker, Multimode 8). The structure of the IGZO films was determined by x-ray photoelectron spectroscopy (XPS, Thermo Scientific, ESCALAB 250). Current–voltage (I–V) characteristics were measured in ambient air using a semiconductor parameter analyzer (Keithley 4200SCS).

RESULTS AND DISCUSSION

Printing of IGZO ink was conducted at fixed temperatures, including nozzle temperature of 25°C and substrate temperature of 40°C. For inks with different concentrations, the droplets were almost consistent, with diameter of about 60 μm, volume of 114 pl, and velocity of 1.8 m/s. Optical microscopy images of IJP-IGZO dots obtained on SiO_2/Si substrate using 0.375 M precursor ink are shown in Fig. 1a and b. There is an obvious "coffee-ring" along the edge of each dot with peak-to-valley height of about 27 nm. Essentially, the cause of coffee rings is inhomogeneous drying of the liquid droplets. Faster evaporation of the solvent along the periphery compared with the interior results in an outward radial capillary flow, carrying solute towards the three-phase contact line during the drying process.[23,24]

Considerable efforts have been devoted to suppress this "coffee-ring" effect. Some effective approaches modulate the solution, e.g., tuning the capillary flow in the droplet or controlling the movement of the three-phase contact line as the droplet evaporates.[25] Using a mixture of high- and
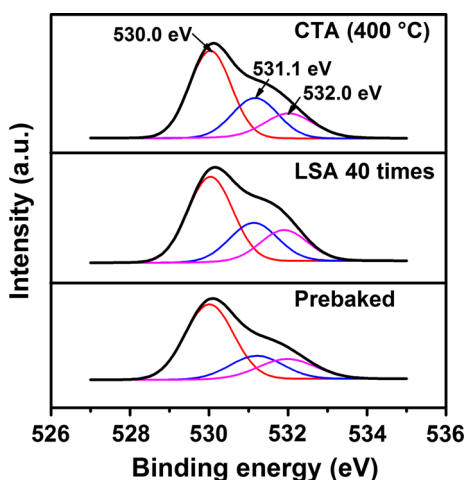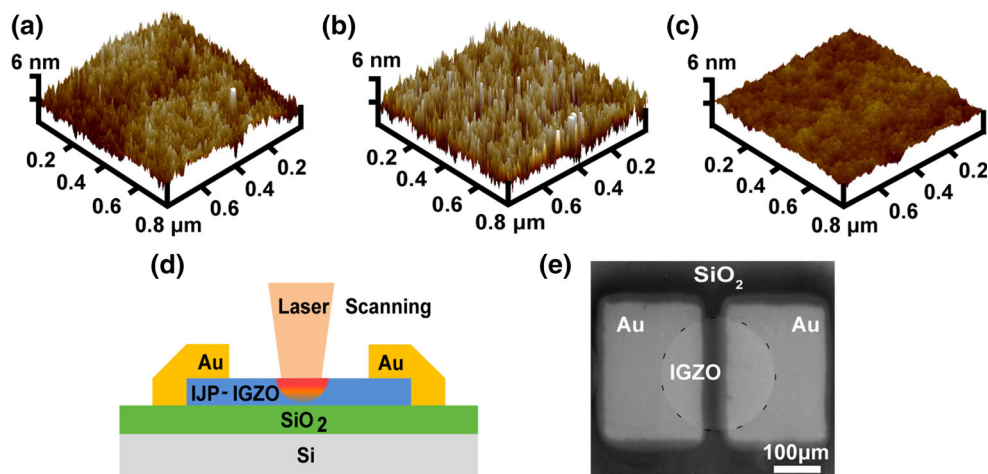

Fig. 3. AFM images of (a) prebaked, (b) LSA-treated, and (c) CTA-treated IGZO thin films. (d) Schematic diagram of device. (e) SEM image of original device.
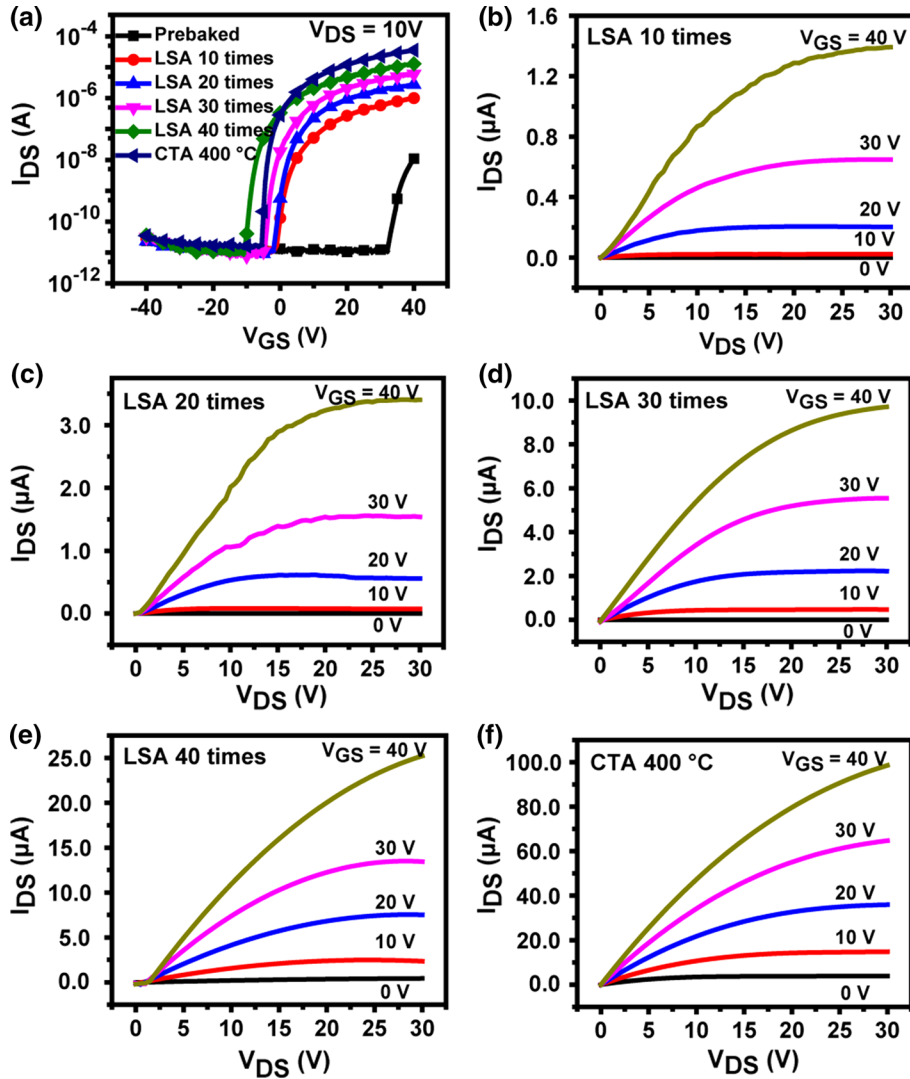
Fig. 4. (a) Transfer characteristics of IJP-IGZO TFTs with LSA and CTA treatments. (b–e) Output curves of IJP-IGZO TFTs treated with LSA for different times. (f) Output curves of IJP-IGZO TFT with CTA at 400°C.

Table III. Electronic parameters of IJP-IGZO TFTs with LSA and CTA treatments

	μ_{FE} (cm^2/V s)	V_{th} (V)	S.S. (V/dec)	$I_{\mathrm{on}}/I_{\mathrm{off}}$
Prebaked	0.004	33	–	9.16×10^2
LSA 10 times	0.07	0	3.43	1.01×10^5
LSA 20 times	0.20	−2	2.09	2.78×10^5
LSA 30 times	0.61	−5	1.91	5.99×10^5
LSA 40 times	1.50	−8.5	1.66	1.29×10^6
CTA (400°C)	1.60	−5	0.94	2.16×10^6

S. S. subthreshold swing

low-boiling-point solvents with different surface tensions, the coffee-ring effect can be effectively minimized.[26] Since use of such mixed solvents induces more complex convection in the droplets, we used a single solvent, even without any stabilizing agent. We found that the concentration of metal precursor had a great effect on the morphology of the printed dots. Use of 1.5 M ink resulted in markedly different IGZO dot arrays, as shown by the microscope images in Fig. 1c and d, where no obvious coffee rings are observed. This result indicates that uniform deposition can be achieved by

Table IV. Comparison of oxide TFTs with LSA treatment from different works

Channel material	Deposition process	Processing temp. (°C)	Laser wavelength (nm)	μ_{FE} (before LSA) (cm^2/V s)	μ_{FE} (after LSA) (cm^2/V s)
IGZO	Inkjet printing	200	1064	0.004	1.50
IGZO nanoparticles[21]	Spin coating	95	355	1.31	7.65
ZnO[35]	Spin coating	95	355	0.19	0.49
ZnO nanoparticles[36]	Spin coating	150	355	–	3.01
IZO[37]	Spin coating	300	248	–	0.25

varying the concentration of metal precursor, being a simple approach in comparison with other, intricate processes. When using techniques to eliminate coffee rings, e.g., surface modification, droplet evaporation usually leads to dome-shaped deposits with thickness that gradually increases from the edge to center.[27] However, Fig. 1d shows coin-like IGZO arrays with steep edges, suggesting that the printing process applied in this work can yield more uniform films. A comparison of the coffee-ring phenomenon between various works is summarized in Table I. Our strategy is facile and efficient for deposition of uniform films. As the concentration was increased from 0.375 M to 1.5 M, the average thickness of the obtained films, regardless of edge rings, varied from 6 nm to 30 nm.

The viscosity and surface tension of inks with different precursor concentrations are presented in Table II. The surface tension increased slightly with increasing amount of dissolved metal salts, while the viscosity changed substantially from 2.52 mPa s (0.375 M) to 8.14 mPa s (1.5 M). It is known that the Marangoni flow of a droplet driven by surface tension gradients can interfere with the outward capillary flow by providing a counterbalance flow. Such surface tension gradients can be caused by concentration gradients (commonly in mixed solutions) or temperature gradients. For the latter, the apex of the printed drop ought to be coolest because it is furthest from the substrate. As the difference in surface tension in Table II is small, the droplets with different concentrations lead to insignificant height difference at the droplet apex, and the temperature field variation between droplets with different concentrations should be negligible. We believe that Marangoni flow is not the key factor in our experiments. On the other hand, higher concentration greatly increased the viscosity, which limits the ability of the solute to diffuse on the substrate and consequently allows formation of uniform films.[23,31]

Figure 2 shows the O 1s XPS spectra of IGZO thin films after different treatments. The curves were fit using three peaks centered at ~530.0 eV, ~531.1 eV, and ~532.0 eV, respectively, which are attributed to oxygen in the stoichiometric oxide lattice, oxygen vacancies, and the presence of loosely bound oxygen impurities such as chemisorbed oxygen, –OH groups, or oxygen interstitials.[32] It can be seen that, after LSA treatment, the oxygen vacancy concentration increased greatly and became nearly comparable to that after conventional thermal annealing. As free electrons in oxide semiconductors arise mainly from generation of oxygen vacancies,[12,33] this implies that the charge carrier concentration after LSA treatment was higher than that in the prebaked thin film.

The surface morphology of IGZO thin films after different treatments was evaluated by atomic force microscopy. The prebaked thin film (Fig. 3a) had rough morphology with root-mean-square (RMS) roughness value of 0.764 nm. After LSA treatment, the RMS roughness increased slightly to 0.895 nm, as shown in Fig. 3b. In contrast, the surface of the film treated by CTA was much smoother with RMS roughness of 0.254 nm. The rapid heating and cooling of LSA is not conducive to formation of smooth surface. A schematic diagram of the device is shown in Fig. 3d, while Fig. 3e shows a SEM image of the original device. The IGZO thin film is indicated by a dashed circle.

The electronic characteristics of IGZO TFTs printed using 1.5 M ink are shown in Fig. 4. The prebaked device, without any posttreatment, showed field-effect mobility of 0.004 cm^2/V s with large positive threshold voltage, V_{th}, of 33 V. After LSA processing, the on-current increased remarkably with the scanning times whereas the off-current remained on the order of 10^{-11} A. The electronic parameters of the devices are summarized in Table III. Both the mobility and on/off current ratio were improved after LSA. V_{th} moved from positive to negative. The shift of V_{th} in the negative direction after high-temperature annealing is mainly due to increased number of oxygen vacancies,[12] which is in accordance with the XPS results in Fig. 2. Huang et al. also demonstrated that V_{th} decreased with increasing carrier concentration in the film.[34]

When scanned 40 times, the field-effect mobility was 1.50 cm^2/V s, more than 300 times larger than that of untreated devices, and an on/off current ratio of 1.29×10^6 was obtained. Conventional thermal annealing was carried out for comparison. The electrical properties of the printed device annealed at 400°C for 3 h are also shown in Fig. 4, exhibiting field-effect mobility of 1.6 cm^2/V s and V_{th} of −5 V.

The effects of LSA are almost comparable to those of long-term high-temperature annealing. Table IV lists the performance of laser-annealed devices from different groups. Compared with spin-coated films, the inkjet-printed film in this work is much thinner. The carrier mobility in the printed film, however, is higher than other amorphous oxides, but lower than films comprising nanoparticles. It is obvious that the NIR laser treatment played a remarkable role in improving the mobility by more than two orders of magnitude.

CONCLUSIONS

We fabricated IGZO TFTs by inkjet printing with low-temperature LSA treatment. Coffee-ring effects were readily solved by modulating the solute concentration in the ink. With increasing precursor concentration, the ink viscosity observably increased, limiting the ability of the solute to diffuse during drying. The influence of rapid LSA on the TFT performance was investigated in detail. The field-effect mobility, threshold voltage, and on/off current ratio were distinctly improved after pulsed laser irradiation. With 40 times laser scanning, printed IGZO TFTs prebaked at temperature as low as 200°C showed mobility of 1.5 cm^2/V s, threshold voltage of -8.5 V, and on/off current ratio $> 10^6$. Rapid LSA treatment therefore represents a promising route toward low-temperature fabrication of solution-processed transparent oxide TFTs, even on flexible substrates.

ACKNOWLEDGEMENTS

REFERENCES

1. T. Kamiya and H. Hosono, *NPG Asia Mater.* 2, 15 (2010).
2. K. Nomura, A. Takagi, T. Kamiya, H. Ohta, M. Hirano, and H. Hosono, *Jpn. J. Appl. Phys.* 45, 4303 (2006).
3. J.S. Park, W.J. Maeng, H.S. Kim, and J.S. Park, *Thin Solid Films* 520, 1679 (2012).
4. K. Nomura, H. Ohta, A. Takagi, T. Kamiya, M. Hirano, and H. Hosono, *Nature* 432, 488 (2004).
5. T. Kamiya, K. Nomura, and H. Hosono, *Sci. Technol. Adv. Mater.* 11, 044305 (2010).
6. H.E. Lee, S. Kim, J. Ko, H. Yeom, C. Byun, S.H. Lee, D.J. Joe, T. Im, S.K. Park, and K.J. Lee, *Adv. Funct. Mater.* 26, 6170 (2016).
7. H. Yabuta, M. Sano, K. Abe, T. Aiba, T. Den, H. Kumomi, K. Nomura, T. Kamiya, and H. Hosono, *Appl. Phys. Lett.* 89, 112123 (2006).
8. S. Jeong, Y.G. Ha, J. Moon, A. Facchetti, and T.J. Marks, *Adv. Mater.* 22, 1346 (2010).
9. J.W. Hennek, Y. Xia, K. Everaerts, M.C. Hersam, A. Facchetti, and T.J. Marks, *ACS Appl. Mater. Interfaces* 4, 1614 (2012).
10. M.L. Xie, S.J. Wu, Z. Chen, Q. Khan, X. Wu, S. Shao, and Z. Cui, *RSC Adv.* 6, 41439 (2016).
11. M. Singh, H.M. Haverinen, P. Dhagat, and G.E. Jabbour, *Adv. Mater.* 22, 673 (2010).
12. S. Hwang, J.H. Lee, C.H. Woo, J.Y. Lee, and H.K. Cho, *Thin Solid Films* 519, 5146 (2011).
13. C.H. Choi, S.Y. Han, Y.W. Su, Z. Fang, L.Y. Lin, C.C. Cheng, and C.H. Chang, *J. Mater. Chem. C* 3, 854 (2015).
14. X.G. Yu, N.J. Zhou, J. Smith, H. Lin, K. Stallings, J.S. Yu, T.J. Marks, and A. Facchetti, *ACS Appl. Mater. Interfaces* 5, 7983 (2013).
15. M.G. Kim, M.G. Kanatzidis, A. Facchetti, and T.J. Marks, *Nat. Mater.* 10, 382 (2011).
16. S.Y. Han, G.S. Herman, and C.H. Chang, *J. Am. Chem. Soc.* 133, 5166 (2011).
17. L.F. Teng, P.T. Liu, Y.J. Lo, and Y.J. Lee, *Appl. Phys. Lett.* 101, 132901 (2012).
18. Y.H. Kim, J.S. Heo, T.H. Kim, S. Park, M.H. Yoon, J. Kim, M.S. Oh, G.R. Yi, Y.Y. Noh, and S.K. Park, *Nature* 489, 128 (2012).
19. Y.S. Rim, W.H. Jeong, D.L. Kim, H.S. Lim, K.M. Kim, and H.J. Kim, *J. Mater. Chem.* 22, 12491 (2012).
20. C.Y. Chung, B. Zhu, D.G. Ast, R.G. Greene, and M.O. Thompson, *Appl. Phys. Lett.* 106, 123506 (2015).
21. Y.-H. Yang, S.S. Yang, and K.-S. Chou, *IEEE Electron Device Lett.* 31, 969 (2010).
22. C.Y. Tsay and T.T. Huang, *Mater. Chem. Phys.* 140, 365 (2013).
23. R.D. Deegan, O. Bakajin, T.F. Dupont, G. Huber, S.R. Nagel, and T.A. Witten, *Nature* 389, 827 (1997).
24. R.D. Deegan, O. Bakajin, T.F. Dupont, G. Huber, S.R. Nagel, and T.A. Witten, *Phys. Rev. E* 62, 756 (2000).
25. M.X. Kuang, L.B. Wang, and Y.L. Song, *Adv. Mater.* 26, 6950 (2014).
26. K.J. Baeg, D. Khim, J.H. Kim, M. Kang, I.K. You, D.Y. Kim, and Y.Y. Noh, *Org. Electron.* 12, 634 (2011).
27. D. Kim, Y. Jeong, K. Song, S.K. Park, G. Cao, and J. Moon, *Langmiur* 25, 11149 (2009).
28. D. Kim, Y. Jeong, C.Y. Koo, K. Song, and J. Moon, *Jpn. J. Appl. Phys.* 49, 05EB06 (2010).
29. S.H. Lee and W.S. Choi, *Electron. Mater. Lett.* 10, 737 (2014).
30. J.S. Lee, Y.J. Kwack, and W.S. Choi, *ACS Appl. Mater. Interfaces* 5, 11578 (2013).
31. J. Fukai, Z. Zhao, D. Poulikakos, C.M. Megaridis, and O. Miyatake, *Phys. Fluids A* 5, 2588 (1993).
32. P. Xiao, L.F. Lan, T. Dong, Z.G. Lin, L. Wang, H.L. Ning, and J.B. Peng, *ECS J. Solid State Sci. Technol.* 3, Q3081 (2014).
33. K. Takechi, M. Nakata, T. Eguchi, H. Yamaguchi, and S. Kaneko, *Jpn. J. Appl. Phys.* 48, 011301 (2009).
34. X.M. Huang, C.F. Wu, H. Lu, F.F. Ren, D.J. Chen, Y.L. Liu, G. Yu, R. Zhang, Y.D. Zheng, and Y.J. Wang, *IEEE Electron Device Lett.* 35, 1034 (2014).
35. Y.-H. Yang, S.S. Yang, and K.-S. Chou, *J. Soc. Inf. Display* 18, 745 (2010).
36. D. Lee, H. Pan, S.H. Ko, H.K. Park, E. Kim, and C.P. Grigoropoulos, *Appl. Phys. A Mater.* 107, 161 (2012).
37. C.N. Chen and J.J. Huang, *J. Appl. Res. Technol.* 13, 170 (2015).